

RESEARCH PAPER



Synthesis and biological evaluation of halogenated phenoxchalcones and their corresponding pyrazolines as cytotoxic agents in human breast cancer

Peter A. Halim^a, Rasha A. Hassan^a, Khaled O. Mohamed^a, Soha O. Hassanin^b, Mona G. Khalil^c, Amr M. Abdou^d and Eman O. Osman^a

^aPharmaceutical Organic Chemistry Department, Faculty of Pharmacy, Cairo University, Cairo, Egypt; ^bBiochemistry Department, Faculty of Pharmacy, Modern University for Technology and Information, Cairo, Egypt; ^cPharmacology and Toxicology Department, Faculty of Pharmacy, Modern University for Technology and Information, Cairo, Egypt; ^dDepartment of Microbiology and Immunology, National Research Centre, Dokki, Egypt

ABSTRACT

Novel halogenated phenoxchalcones **2a–f** and their corresponding *N*-acetylpyrazolines **3a–f** were synthesised and evaluated for their anticancer activities against breast cancer cell line (MCF-7) and normal breast cell line (MCF-10a), compared with staurosporine. All compounds showed moderate to good cytotoxic activity when compared to control. Compound **2c** was the most active, with $IC_{50} = 1.52 \mu M$ and selectivity index = 15.24. Also, chalcone **2f** showed significant cytotoxic activity with $IC_{50} = 1.87 \mu M$ and selectivity index = 11.03. Compound **2c** decreased both total mitogen activated protein kinase (p38 α MAPK) and phosphorylated enzyme in MCF-7 cells, suggesting its ability to decrease cell proliferation and survival. It also showed the ability to induce ROS in MCF-7 treated cells. Compound **2c** exhibited apoptotic behaviour in MCF-7 cells due to cell accumulation in G2/M phase and elevation in late apoptosis 57.78-fold more than control. Docking studies showed that compounds **2c** and **2f** interact with p38 α MAPK active sites.

ARTICLE HISTORY

Received 5 August 2021
Revised 19 October 2021
Accepted 19 October 2021

KEYWORDS

Halogenated chalcones; diaryl ether; pyrazoline; ROS; p38 MAPK; breast cancer; cell cycle profile

1. Introduction

There is a continuous effort in the field of synthetic medicinal chemistry to develop new molecules with better activity and safety profile¹. Different scaffolds are continuously evaluated for their anticancer activity in the hope to overcome the side effects and improve bioavailability^{2–6}. Breast cancer is one of the most common forms of invasive cancer in women. It is considered the most commonly diagnosed cancer and one of the leading causes of death among women⁷. Breast cancer is responsible for 16.2% of all female cancers and 22.9% of invasive cancers in women. It also accounts for 18.2% of all cancer deaths worldwide⁸.

Chalcones are considered as a subclass of flavonoids and they are broadly displayed in plants such as vegetables and tea⁹. They are utilised as both biosynthetic precursors of flavonoids and as end products as well⁹. Chalcones have shown different pharmacological activities including acetylcholinesterase inhibition¹⁰, anti-inflammatory¹¹, antimicrobial¹², antihyperlipidemic¹³, and anticancer activities^{14–16}.

The modification of chalcone scaffold to improve their bioavailability and anticancer activity has grabbed the attention of many authors. The diaryl ether scaffold is commonly found in many natural products and biologically essential molecules^{17–19}. Research has shown that chalcones with a diaryl ether nucleus (**I–V**, Figure 1) possess effective cytotoxic activity including derivatives with high selectivity against breast cancer cell lines such as MCF-7 cell^{20–22}. Some diaryl ether chalcones were found to express their cytotoxic activity through inhibition of tubulin polymerisation^{20,21}.

Various dihalogenated chalcones have been of interest as intermediates in the synthesis of flavones and chromones^{23,24}. Halogenated chalcones (**II–X**, Figure 1) have been reported to exhibit high cytotoxic activity^{25–28}. They were also reported to be effective against leukaemia cell lines^{15,29} and against breast cancer cell line^{15,30–32}.

Many chalcones have the ability to inhibit tumour proliferation by a variety of mechanisms as inhibition of tubulin²⁰, epidermal growth factor receptor (EGFR)³³, vascular endothelial growth factor receptor-2 (VEGFR-2)^{5,15} and mitogen-activated protein kinase (MAPK)^{29,34}.

MAPKs are vital elements for intracellular transmission of signals regulating many cell functions. p38 MAPK has been demonstrated to play a major role in cell survival, proliferation, differentiation, and apoptosis in mammalian cells³⁵. It was reported that the ability of chalcones to induce cell cycle arrest and apoptosis would be due to down-regulation of p38 MAPK and inhibition of its phosphorylation³⁶. Targeting p38 MAPK through its inhibition or down-regulation is considered as an important strategy in the search for new anticancer molecules.

The objective of the current research was to design and synthesise a series of chalcones with hybridisation of halogenated chalcones and diaryl ether moiety **2a–f** (Figure 2). We planned to cyclize the synthesised chalcones to their corresponding *N*-acetylpyrazolines **3a–f** (Figure 2) as inspired by literature survey of possible anticancer activity of this scaffold³⁷. We also planned to test

CONTACT Rasha A. Hassan  rasha.hasan@pharma.cu.edu.eg  Pharmaceutical Organic Chemistry Department, Faculty of Pharmacy, Cairo University, Cairo 11562, Egypt

© 2021 The Author(s). Published by Informa UK Limited, trading as Taylor & Francis Group.

This is an Open Access article distributed under the terms of the Creative Commons Attribution License (<http://creativecommons.org/licenses/by/4.0/>), which permits unrestricted use, distribution, and reproduction in any medium, provided the original work is properly cited.

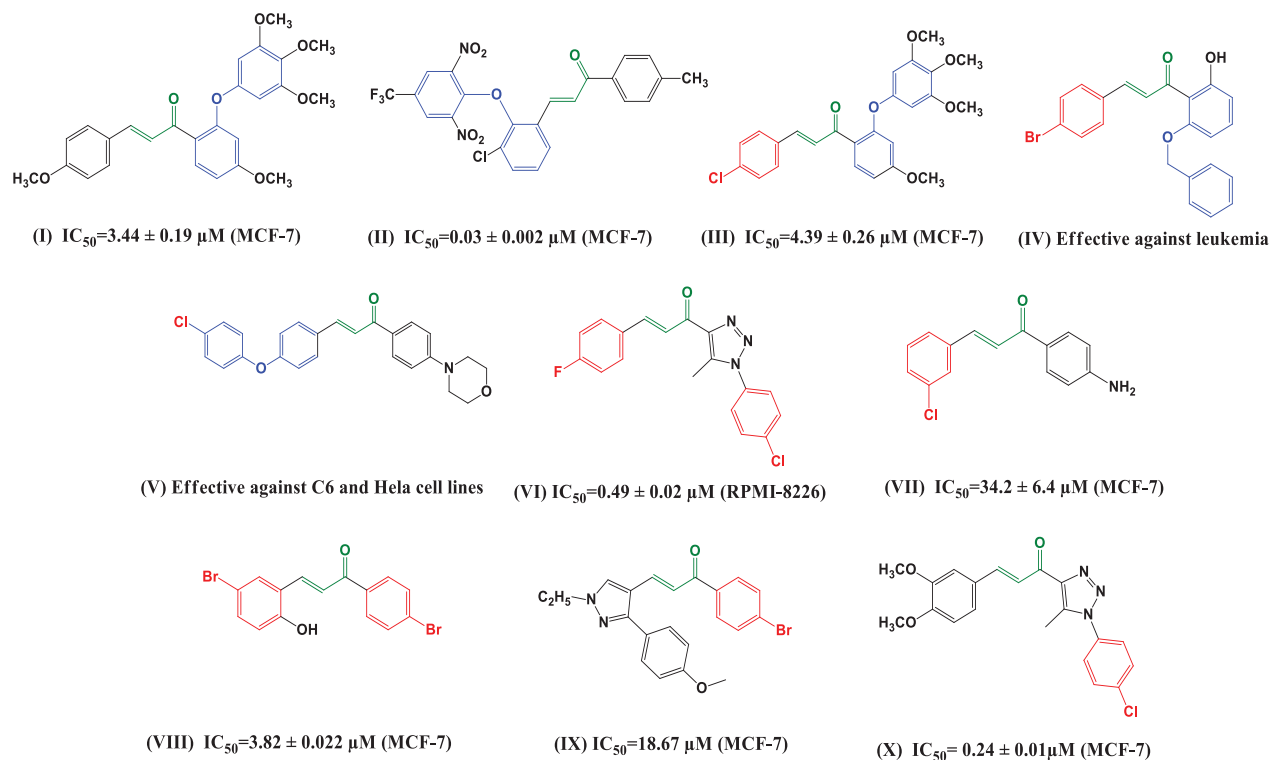


Figure 1. Structures of some reported diaryl ether chalcones I–V and halogenated chalcones II–X with cytotoxic activity.

the anticancer activity of the synthesised compounds against breast cancer.

Materials and methods

Chemistry

General

Melting points were obtained on a Griffin apparatus and were uncorrected. Microanalyses for C, H and N were carried out at the Regional Centre for Mycology and Biotechnology, Faculty of Pharmacy, Al-Azhar University. IR spectra were recorded on Shimadzu IR 435 spectrophotometer (Shimadzu Corp., Kyoto, Japan) Faculty of Pharmacy, Cairo University, Cairo, Egypt and values were represented in cm^{-1} . ^1H NMR spectra were carried out on Bruker 400 MHz (Bruker Corp., Billerica, MA, USA) spectrophotometer, Faculty of Pharmacy, Cairo University, Cairo, Egypt. Chemical shifts were recorded in ppm on δ scale, coupling constants (J) were given in Hz and peak multiplicities were designed as follows: s, singlet; d, doublet; dd, doublet of doublets; t, triplet; m, multiplet ^{13}C NMR spectra were carried out on Bruker 100 MHz spectrophotometer, Faculty of Pharmacy, Cairo University, Cairo, Egypt. Progress of the reactions were monitored by TLC using pre-coated aluminium sheet silica gel MERCK 60F 254 and was visualised by UV lamp. Compounds **1a,b** were previously reported in the literature³⁸ and they were prepared in this work according to the reported procedure³⁹.

General procedure for the preparation of the phenoxychalcones 2a–f

To an ice cooled, stirred solution of 4-(4-substitutedphenoxy)benzaldehyde (**1a,b**) (0.01 mol) and 4-substituted acetophenone (0.01 mol) in 95% ethanol, 40% aqueous KOH solution was added portion wise. Stirring was continued for 5 h. Solid product was

filtered and washed with 3% aqueous HCl and crystallised from ethanol.

3-(4-(4-Bromophenoxy)phenyl)-1-(4-chlorophenyl)prop-2-en-1-one (2a). Yellow solid: 86% yield; mp 150–152 °C; IR (KBr, cm^{-1}) 3086 (CH aromatic), 1658 (C=O), 1608 (C=C); ^1H NMR (400 MHz, DMSO- d_6) δ 8.18 (d, $J=8.4$ Hz, 2H, ArH), 7.95 (d, $J=8.4$ Hz, 2H, ArH), 7.88 (d, $J=15.7$ Hz, 1H, CH=CH-CO), 7.76 (d, $J=15.7$ Hz, 1H, CH=CH-CO), 7.66–7.60 (m, 4H, ArH), 7.11–7.06 (m, 4H, ArH); ^{13}C NMR (100 MHz, DMSO- d_6) δ 188.4, 158.9, 155.7, 144.2, 138.5, 136.7, 133.5, 131.6, 130.9, 130.6, 129.3, 121.9, 121.3, 119.1, 116.4; Anal. Calcd for $\text{C}_{21}\text{H}_{14}\text{BrClO}_2$ (413.69): C, 60.97; H, 3.41, found C, 60.33; H, 3.65.

3-(4-(4-Bromophenoxy)phenyl)-1-(4-bromophenyl)prop-2-en-1-one (2b). Yellow solid: 82% yield; mp 164–166 °C; IR (KBr, cm^{-1}) 3086 (CH aromatic), 1658 (C=O), 1612, (C=C); ^1H NMR (400 MHz, DMSO- d_6) δ 8.09 (d, $J=8.4$ Hz, 2H, ArH), 7.95 (d, $J=8.4$ Hz, 2H, ArH), 7.87 (d, $J=15.6$ Hz, 1H, CH=CH-CO), 7.80–7.74 (m, 3H, 2ArH + CH=CH-CO), 7.61 (d, $J=8.4$ Hz, 2H, ArH), 7.11–7.06 (m, 4H, ArH); ^{13}C NMR (100 MHz, DMSO- d_6) δ 188.7, 159.0, 155.7, 144.3, 137.1, 133.5, 132.3, 131.6, 131.0, 130.6, 127.7, 121.9, 121.3, 119.1, 116.4; Anal. Calcd for $\text{C}_{21}\text{H}_{14}\text{Br}_2\text{O}_2$ (458.14): C, 55.05; H, 3.08, found C, 54.81 H, 3.52.

3-(4-(4-Bromophenoxy)phenyl)-1-(p-tolyl)prop-2-en-1-one (2c). Yellow solid: 90% yield; mp 157–159 °C; IR (KBr, cm^{-1}) 3089 (CH aromatic), 1658 (C=O), 1600, (C=C); ^1H NMR (400 MHz, DMSO- d_6) δ 8.07 (d, $J=8.0$ Hz, 2H, ArH), 7.94 (d, $J=8.4$ Hz, 2H, ArH), 7.87 (d, $J=15.6$ Hz, 1H, CH=CH-CO), 7.73 (d, $J=15.6$ Hz, 1H, CH=CH-CO), 7.60 (d, $J=8.4$ Hz, 2H, ArH), 7.38 (d, $J=8.0$ Hz, 2H, ArH), 7.10–7.05 (m, 4H, ArH), 2.41 (s, 3H, CH_3); ^{13}C NMR (100 MHz, DMSO- d_6) δ 189.0, 158.7, 155.8, 144.0, 143.3, 135.6, 133.4, 131.5, 130.8, 129.8, 129.1, 121.8, 121.7, 119.1, 116.3, 21.7; Anal. Calcd for $\text{C}_{22}\text{H}_{17}\text{BrO}_2$ (393.27): C, 67.19; H, 4.36, found C, 67.64; H, 4.43.

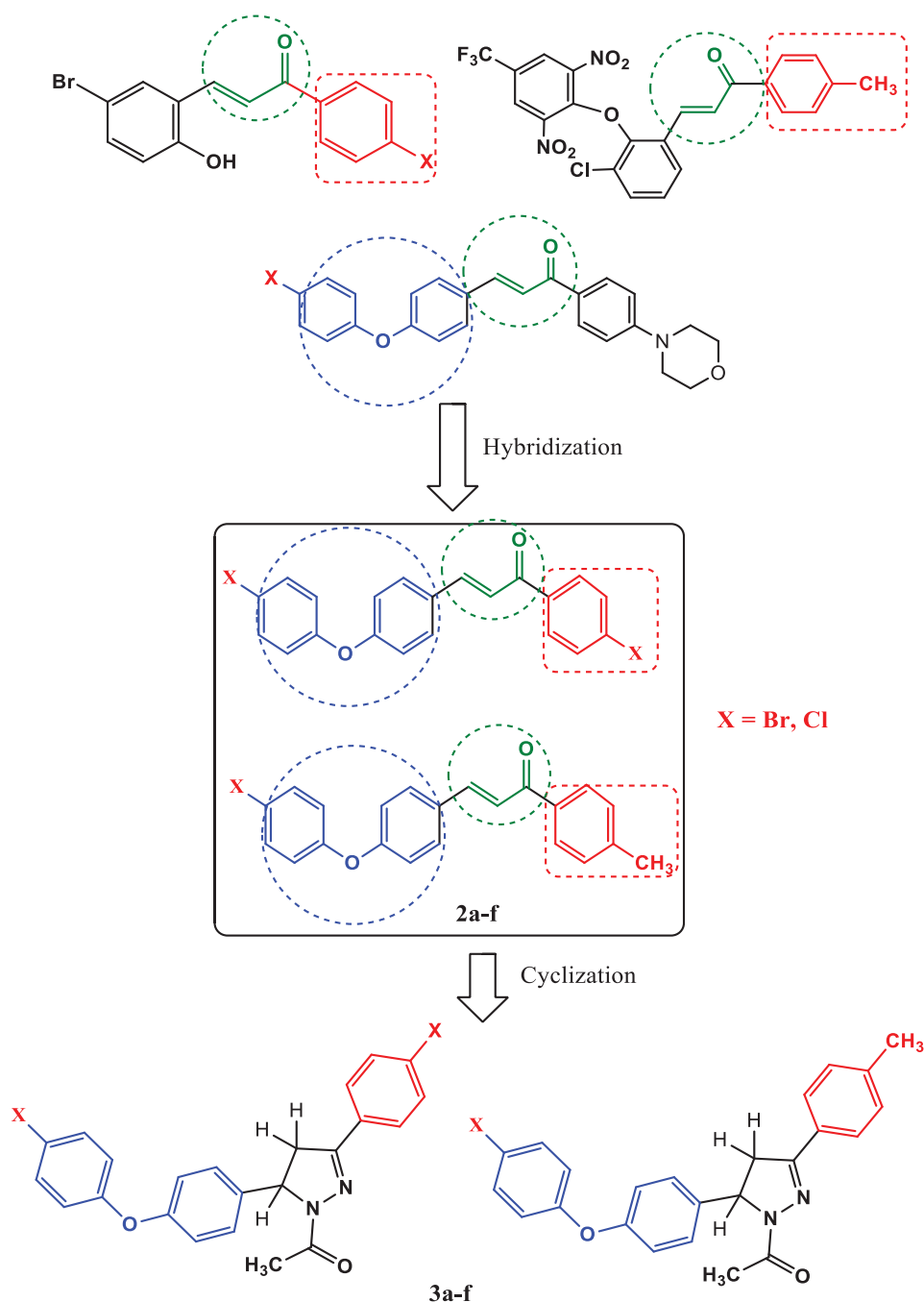


Figure 2. Molecular hybridisation of halogenated chalcones and diaryl ether chalcones to yield the designed chalcones **2a-f** and *N*-acetylpyrazoline derivatives **3a-f** upon cyclisation.

3-(4-(4-Chlorophenoxy)phenyl)-1-(4-chlorophenyl)prop-2-en-1-one (2d). Yellow solid: 83% yield; mp 120–122 °C; IR (KBr, cm^{-1}) 3089 (CH aromatic), 1658 (C=O), 1608, (C=C); ^1H NMR (400 MHz, DMSO-d_6) δ 8.18 (d, $J=8.4$ Hz, 2H, ArH), 7.95 (d, $J=8.4$ Hz, 2H, ArH), 7.88 (d, $J=15.6$ Hz, 1H, $\text{CH}=\text{CH-CO}$), 7.76 (d, $J=15.6$ Hz, 1H, $\text{CH}=\text{CH-CO}$), 7.65 (d, $J=8.4$ Hz, 2H, ArH), 7.48 (d, $J=8.4$ Hz, 2H, ArH), 7.14–7.08 (m, 4H, ArH); ^{13}C NMR (100 MHz, DMSO-d_6) δ 188.4, 159.1, 155.1, 144.2, 138.5, 136.7, 131.6, 130.8, 130.5, 130.5, 129.3, 128.5, 121.5, 121.2, 118.9; Anal. Calcd for $\text{C}_{21}\text{H}_{14}\text{Cl}_2\text{O}_2$ (369.24): C, 68.31; H, 3.82, found C, 67.72; H, 4.11.

1-(4-Bromophenyl)-3-(4-(4-chlorophenoxy)phenyl)prop-2-en-1-one (2e). Yellow solid: 79% yield; mp 143–145 °C; IR (KBr, cm^{-1}) 3089 (CH aromatic), 1658 (C=O), 1608, (C=C); ^1H NMR (400 MHz,

DMSO-d_6) δ 8.09 (d, $J=8.4$ Hz, 2H, ArH), 7.94 (d, $J=8.4$ Hz, 2H, ArH), 7.87 (d, $J=15.6$ Hz, 1H, $\text{CH}=\text{CH-CO}$), 7.80–7.74 (m, 3H, ArH, $\text{CH}=\text{CH-CO}$), 7.48 (d, $J=8.4$ Hz, 2H, ArH), 7.14–7.08 (m, 4H, ArH); ^{13}C NMR (100 MHz, DMSO-d_6) δ 188.7, 159.1, 155.1, 144.3, 137.1, 132.3, 131.6, 131.0, 130.5, 130.5, 128.5, 127.7, 121.5, 121.2, 118.9; Anal. Calcd for $\text{C}_{21}\text{H}_{14}\text{BrClO}_2$ (413.69): C, 60.97; H, 3.41, found C, 60.63; H, 3.78.

3-(4-(4-Chlorophenoxy)phenyl)-1-(p-tolyl)prop-2-en-1-one (2f). Yellow solid: 86% yield; mp 136–138 °C; IR (KBr, cm^{-1}) 3089 (CH aromatic), 1658 (C=O), 1600 (C=C); ^1H NMR (400 MHz, DMSO-d_6) δ 8.07 (d, $J=8.0$ Hz, 2H, ArH), 7.93 (d, $J=8.0$ Hz, 2H, ArH), 7.87 (d, $J=15.6$ Hz, 1H, $\text{CH}=\text{CH-CO}$), 7.73 (d, $J=15.6$ Hz, 1H, $\text{CH}=\text{CH-CO}$), 7.48 (d, $J=8.0$ Hz, 2H, ArH), 7.38 (d, $J=8.0$ Hz, 2H, ArH), 7.14–7.07

(m, 4H, ArH), 2.41 (s, 3H, CH₃); ¹³C NMR (100 MHz, DMSO-d₆) δ: 189.0, 158.9, 155.2, 144.0, 143.3, 135.6, 131.4, 130.7, 130.5, 129.8, 129.1, 128.4, 121.7, 121.4, 119.0, 21.7; Anal. Calcd for C₂₂H₁₇ClO₂ (348.82): C, 75.75; H, 4.91, found C, 76.08; H, 4.68.

General procedure for the preparation of substituted 4,5-dihydro-1H-pyrazol-1-yl)ethan-1-one (3a–f)

A mixture of phenoxychalcones **2a–f** (1.0 mmol), hydrazine hydrate (5.0 mmol) and acetic acid (5.0 ml) was heated under reflux for 3 h. The reaction mixture was cooled and poured onto crushed ice. Solid product was filtered, washed with water and crystallised from ethanol.

1-(5-(4-(4-Bromophenoxy)phenyl)-3-(4-chlorophenyl)-4,5-dihydro-1H-pyrazol-1-yl) ethanone (3a). White solid: 89% yield; mp 142–144 °C; IR (KBr, cm⁻¹) 3051 (CH aromatic), 2943, 2927 (CH aliphatic), 1658 (C=O), 1593 (C=N); ¹H NMR (400 MHz, DMSO-d₆) δ 7.80 (d, *J* = 8.0 Hz, 2H, ArH), 7.55–7.52 (m, 4H, ArH), 7.23 (d, *J* = 8.0 Hz, 2H, ArH), 6.99 (d, *J* = 8.4 Hz, 2H, ArH), 6.94 (d, *J* = 8.4 Hz, 2H, ArH), 5.56 (dd, *J* = 12.0, 4.4 Hz, 1H, H_X pyrazoline), 3.85 (dd, *J* = 18.4, 12.0 Hz, 1H, H_B pyrazoline), 3.16 (dd, *J* = 18.4, 4.4 Hz, 1H, H_A pyrazoline), 2.31 (s, 3H, CH₃CO); ¹³C NMR (100 MHz, DMSO-d₆) δ 168.1, 156.6, 155.6, 153.7, 138.3, 135.4, 133.2, 130.4, 129.3, 128.8, 127.8, 121.0, 119.5, 115.5, 59.6, 42.4, 22.2; Anal. Calcd for C₂₃H₁₈BrClN₂O₂ (469.76): C, 58.81; H, 3.86; N, 5.96, found C, 58.57; H, 3.61; N, 6.12.

1-(5-(4-(4-Bromophenoxy)phenyl)-3-(4-bromophenyl)-4,5-dihydro-1H-pyrazol-1-yl) ethanone (3b). White solid: 85% yield; mp 138–140 °C; IR (KBr, cm⁻¹) 3051 (CH aromatic), 2974, 2924 (CH aliphatic), 1658 (C=O), 1589 (C=N); ¹H NMR (400 MHz, DMSO-d₆) δ 7.73 (d, *J* = 8.4 Hz, 2H, ArH), 7.67 (d, *J* = 8.4 Hz, 2H, ArH), 7.54 (d, *J* = 8.4 Hz, 2H, ArH), 7.22 (d, *J* = 8.4 Hz, 2H, ArH), 7.00–6.94 (m, 4H, ArH), 5.56 (dd, *J* = 11.8, 4.6 Hz, 1H, H_X pyrazoline), 3.85 (dd, *J* = 18.2, 11.8 Hz, 1H, H_B pyrazoline), 3.16 (dd, *J* = 18.2, 4.6 Hz, 1H, H_A pyrazoline), 2.31 (s, 3H, CH₃CO); ¹³C NMR (100 MHz, DMSO-d₆) δ 168.0, 156.6, 155.6, 153.8, 138.3, 133.2, 132.2, 130.8, 129.0, 127.9, 124.1, 121.0, 119.5, 115.5, 59.6, 42.4, 22.2; Anal. Calcd for C₂₃H₁₈Br₂N₂O₂ (514.21): C, 53.72; H, 3.53; N, 5.45, found C, 53.51; H, 3.28; N, 5.69.

1-(5-(4-(4-Bromophenoxy)phenyl)-3-(p-tolyl)-4,5-dihydro-1H-pyrazol-1-yl)ethanone (3c). White solid: 92% yield; mp 141–143 °C; IR (KBr, cm⁻¹) 3050 (CH aromatic), 2947, 2920 (CH aliphatic), 1662 (C=O), 1585 (C=N); ¹H NMR (400 MHz, DMSO-d₆) δ 7.68 (d, *J* = 8.0 Hz, 2H, ArH), 7.54 (d, *J* = 8.4 Hz, 2H, ArH), 7.28 (d, *J* = 8.0 Hz, 2H, ArH), 7.22 (d, *J* = 8.4 Hz, 2H, ArH), 6.99 (d, *J* = 8.4 Hz, 2H, ArH), 6.95 (d, *J* = 8.4 Hz, 2H, ArH), 5.54 (dd, *J* = 12.0, 4.4 Hz, 1H, H_X pyrazoline), 3.83 (dd, *J* = 18.0, 12.0 Hz, 1H, H_B pyrazoline), 3.12 (dd, *J* = 18.0, 4.4 Hz, 1H, H_A pyrazoline), 2.35 (s, 3H, CH₃CO), 2.30 (s, 3H, CH₃); ¹³C NMR (100 MHz, DMSO-d₆) δ 167.8, 156.6, 155.6, 154.6, 140.6, 138.5, 133.2, 129.8, 128.8, 127.8, 127.1, 121.0, 119.5, 115.5, 59.2, 42.6, 22.2, 21.5; Anal. Calcd for C₂₄H₂₁BrN₂O₂ (449.34): C, 64.15; H, 4.71; N, 6.23, found C, 64.43; H, 4.62; N, 6.34.

1-(5-(4-(4-Chlorophenoxy)phenyl)-3-(4-chlorophenyl)-4,5-dihydro-1H-pyrazol-1-yl) ethanone (3d). White solid: 81% yield; mp 116–118 °C; IR (KBr, cm⁻¹) 3043 (CH aromatic), 2978, 2924 (CH aliphatic), 1658 (C=O), 1593 (C=N); ¹H NMR (400 MHz, DMSO-d₆) δ 7.81 (d, *J* = 8.4 Hz, 2H, ArH), 7.54 (d, *J* = 8.4 Hz, 2H, ArH), 7.42 (d,

J = 8.4 Hz, 2H, ArH), 7.22 (d, *J* = 8.4 Hz, 2H, ArH), 7.02–6.98 (m, 4H, ArH), 5.56 (dd, *J* = 12.0, 4.4 Hz, 1H, H_X pyrazoline), 3.85 (dd, *J* = 18.0, 12.0 Hz, 1H, H_B pyrazoline), 3.16 (dd, *J* = 18.0, 4.4 Hz, 1H, H_A pyrazoline), 2.31 (s, 3H, CH₃CO); ¹³C NMR (100 MHz, DMSO-d₆) δ 168.0, 156.1, 155.8, 153.7, 138.3, 135.3, 130.5, 130.3, 129.3, 128.8, 127.9, 127.6, 120.6, 119.4, 59.6, 42.4, 22.2; Anal. Calcd for C₂₃H₁₈Cl₂N₂O₂ (425.31): C, 64.95; H, 4.27; N, 6.59, found C, 65.18; H, 4.02; N, 6.87

1-(3-(4-Bromophenyl)-5-(4-(4-chlorophenoxy)phenyl)-4,5-dihydro-1H-pyrazol-1-yl) ethanone (3e). White solid: 80% yield; mp 117–119 °C; IR (KBr, cm⁻¹) 3050 (CH aromatic), 2945, 2920 (CH aliphatic), 1658 (C=O), 1585 (C=N); ¹H NMR (400 MHz, DMSO-d₆) δ 7.73 (d, *J* = 8.4 Hz, 2H, ArH), 7.67 (d, *J* = 8.8 Hz, 2H, ArH), 7.42 (d, *J* = 8.8 Hz, 2H, ArH), 7.22 (d, *J* = 8.8 Hz, 2H, ArH), 7.02–6.98 (m, 4H, ArH), 5.56 (dd, *J* = 12.0, 4.4 Hz, 1H, H_X pyrazoline), 3.85 (dd, *J* = 18.0, 12.0 Hz, 1H, H_B pyrazoline), 3.16 (dd, *J* = 18.0, 4.4 Hz, 1H, H_A pyrazoline), 2.31 (s, 3H, CH₃CO); ¹³C NMR (100 MHz, DMSO-d₆) δ 168.0, 156.1, 155.8, 153.8, 138.3, 132.2, 130.8, 130.3, 129.0, 127.9, 127.6, 124.1, 120.6, 119.4, 59.6, 42.4, 22.2; Anal. Calcd for C₂₃H₁₈BrClN₂O₂ (469.76): C, 58.81; H, 3.86; N, 5.96, found C, 59.13; H, 3.55; N, 5.73.

1-(5-(4-(4-Chlorophenoxy)phenyl)-3-(p-tolyl)-4,5-dihydro-1H-pyrazol-1-yl) ethanone (3f). Yellow solid: 88% yield; mp 118–120 °C; IR (KBr, cm⁻¹) 3039 (CH aromatic), 2947, 2920 (CH aliphatic), 1658 (C=O), 1589 (C=N); ¹H NMR (400 MHz, DMSO-d₆) δ 7.69 (d, *J* = 8.0 Hz, 2H, ArH), 7.42 (d, *J* = 8.8 Hz, 2H, ArH), 7.28 (d, *J* = 8.0 Hz, 2H, ArH), 7.22 (d, *J* = 8.8 Hz, 2H, ArH), 7.02–6.98 (m, 4H, ArH), 5.54 (dd, *J* = 12.0, 4.4 Hz, 1H, H_X pyrazoline), 3.84 (dd, *J* = 18.0, 12.0 Hz, 1H, H_B pyrazoline), 3.13 (dd, *J* = 18.0, 4.4 Hz, 1H, H_A pyrazoline), 2.35 (s, 3H, CH₃CO), 2.30 (s, 3H, CH₃); ¹³C NMR (100 MHz, DMSO-d₆) δ 167.8, 156.1, 155.7, 154.6, 140.6, 138.4, 130.3, 129.8, 128.8, 127.8, 127.6, 127.1, 120.6, 119.4, 59.2, 42.6, 22.2, 21.5; Anal. Calcd for C₂₄H₂₁ClN₂O₂ (404.89): C, 71.19; H, 5.23; N, 6.92, found C, 71.45; H, 5.56; N, 6.61.

Biological evaluation

Chemicals

General anticancer assessment using MTT assay

Cell Culture. Human breast cancer cell line MCF-7 and normal breast cell line MCF-10a were obtained from American type culture collection, MCF-7 cells were cultured using Dulbecco's Modified Eagle Medium DMEM (Invitrogen/Life Technologies) supplemented with 10% FBS (Hyclone), 10 µg/ml of insulin (Sigma), and 1% penicillin-streptomycin. MCF-10a cell line was cultured using DMEM medium supplemented with 10% FBS, 1% sodium pyruvate, 1% MEM NEAA, 20 ng/ml human epidermal growth factor (HEGF), 10 µg/ml insulin and 0.05 mM hydrocortisone. The cells were incubated at 37 °C in a humidified atmosphere of 5% CO₂.

MTT assay

The anticancer effect of phenoxychalcones and *N*-acetylpyrazolines on the viability of both tumour and normal cells was evaluated using MTT assay as a rapid colorimetric assay. It is based on the ability of mitochondrial dehydrogenases of viable cells to reduce yellow tetrazolium salt MTT to blue formazan in quantities proportional to the number of living cells⁴⁰. The cells were incubated with the medium alone or with the tested compounds at concentrations of 100 µM, 25 µM, 6.25 µM, 1.56 µM and 0.39 µM for 48 h.

Staurosporine tested for 48 h of incubation served as positive control. Then, 20 μL MTT solution was added to each well and mixed. After 4 h, the supernatants were removed and 100 μL DMSO was added to each well to dissolve the precipitate. The viability of cells was estimated by measuring the absorbance at 570 nm using a Biotek ELISA plate reader. The cell viability percentage was calculated based on the absorbance ratio between cell culture treated with the compounds and the untreated control multiplied by 100. Selectivity index (SI) was calculated as the ratio of cytotoxicity (IC_{50}) on normal cells (MCF-10a) to cancer cells (MCF-7).

Cell cycle analysis

The cell cycle analysis was carried out by flow cytometry using ab139418_propidium iodide flow cytometry kit/BD (Abcam, Cambridge, UK) according to the manufacturer instructions. Briefly, MCF-7 cells were treated with compound **2c** at its IC_{50} concentration for 24 h. After treatment, the cells were washed twice with ice-cold phosphate buffer saline (PBS) and collected by centrifugation. The cells were then fixed using ice-cold 66% (v/v) ethanol, washed with PBS, and re-suspended with 0.1 mg/mL RNase to digest cellular RNA and thus minimise stained RNA in the background. The cells were then stained with 40 mg/mL propidium iodide (PI), a fluorescent molecule with the ability to bind to nucleic acid. PI binds to the DNA in cells in proportion to its amount. As the DNA content is different among cells in different phases of cell cycle, the stage of cell growth can be determined based on fluorescence intensity. Cell fluorescence was evaluated using FACS Calibur (BD Biosciences, USA) and analysed using CellQuest software (Becton Dickinson)⁴¹. Cell cycle analysis of MCF-7 cells without any treatment was used as control.

Detection of apoptosis

Apoptosis assessment was carried out by flow cytometry using Annexin V-FITC and propidium iodide double-staining apoptosis detection kit (Biovision, USA) according to the manufacturer instructions. Annexin V is a protein with high affinity for phosphatidylserine (PS). The latter is a cell membrane component that translocate from the inner face of the plasma membrane to the cell surface soon after initiating apoptosis. Once on the cell surface, PS can be detected by fluorescent conjugate of Annexin V. Briefly, 5×10^5 MCF-7 cells were treated with compound **2c** at its IC_{50} concentration for 24 h. The cells were then collected by centrifugation and re-suspended in 500 μL of binding buffer. Annexin V-FITC and PI double staining was performed by adding 5 μL of Annexin V-FITC and 5 μL of PI. The cells were then incubated in dark, at room temperature for 5 min. After incubation, cell fluorescence was evaluated using FACS Calibur (BD Biosciences, USA). Dot-plot graphs were used to illustrate the results.

Intracellular reactive oxygen species (ROS) analysis

Intracellular ROS was detected by cell-permeable fluorogenic probe H₂DCFDA. Cell culture subdivided into three groups. The groups are the negative control (untreated MCF-7 cells), the positive control group (MCF-7 cells treated with H₂O₂), and test group (MCF-7 cells treated with compound **2c**). After removing the culture supernatants, the cells were then incubated in fresh medium with 10 μM H₂DCFDA at the dark at 37 °C for 1 h. The cells were washed with PBS buffer, then, harvested and the pellets were suspended in PBS. Samples were analysed ROBOTIK P2000 ELISA reader wavelength 450 nm.

p38 MAPK (phosphorylated and total)

Measurements were performed using ELISA kits (R&D systems, Minneapolis, MN, USA ELISA (Cat. # KHO0071) and p38 MAPK (Total) ELISA, according to the manufacturer's instructions.

Molecular docking in the active site of p38alpha MAP kinase

All the molecular modelling studies were carried out using Molecular Operating Environment (MOE, 2019.0102) software. All minimizations were performed with MOE until an RMSD gradient of 0.1 kcal·mol⁻¹·Å⁻¹ with MMFF94x force field and the partial charges were automatically calculated. The X-ray crystallographic structure of p38alpha MAP Kinase complexed with [5-amino-1-(4-fluorophenyl)-1H-pyrazol-4-yl][3-(piperidin-4-yloxy)phenyl]methanone (PQA) ligand (PDB ID: 2BAL)⁴² was downloaded from the protein data bank⁴³. For each co-crystallised enzyme; water molecules and ligands which are not involved in the binding were removed, the protein was prepared for the docking study using Protonate 3D protocol in MOE with default options. The co-crystallized ligand (PQA) was used to define the binding site for docking. Triangle matcher placement method and London dG scoring function were used for docking.

Statistical analysis

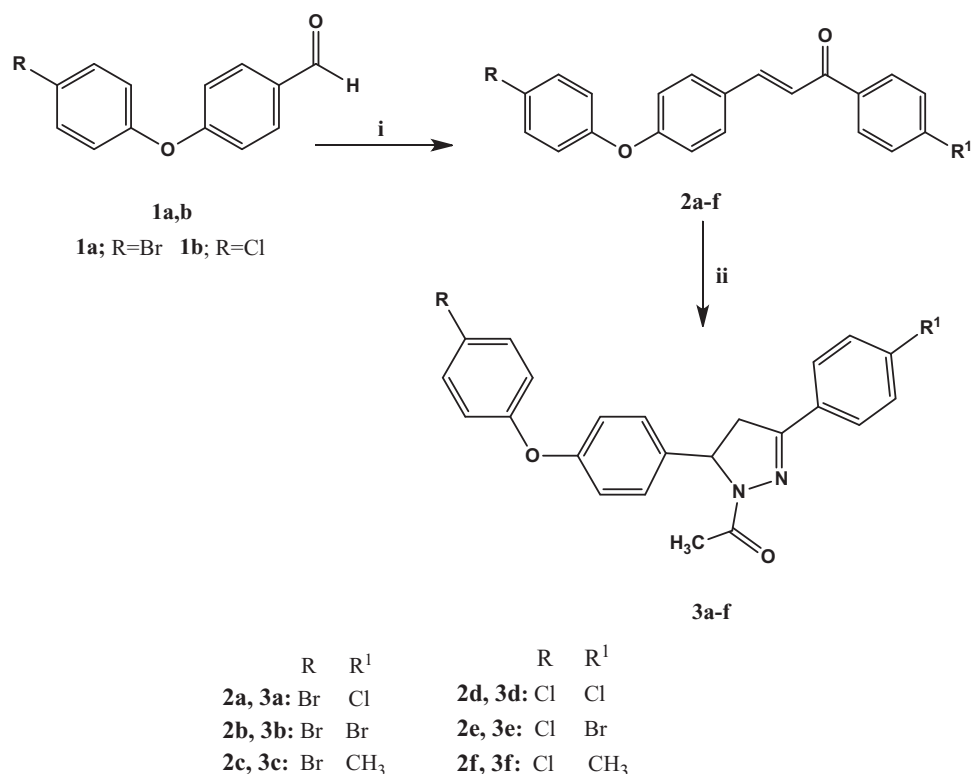
Data are represented as mean \pm SD. Significant differences between groups were analysed by using one-way ANOVA with post-hoc comparisons using Tukey's test (SPSS v18, Chicago, IL, USA). Differences were considered significant at $p < 0.05$.

Results and discussion

Chemistry

Novel halogenated phenoxychalcones **2a-f** and their corresponding *N*-acetylpyrazolines **3a-f** were synthesised according to Scheme 1. Phenoxybenzaldehydes were previously prepared by reacting 4-nitrobenzaldehyde and phenylboronic acid using rhodium catalyst and CsCO₃ as a base³⁸. However, in this research phenoxybenzaldehydes **1a,b** were prepared via Williamson etherification of 4-substituted phenols and 4-fluorobenzaldehyde according to a reported method³⁹. A series of 1,3-diaryl-2-propen-1-ones **2a-f** was obtained via reacting compounds **1a,b** with different 4-substituted acetophenones under base catalysed Claisen-Schmidt condensation^{44,45} in a good to excellent yield (79–90%). The structures of compounds **2a-f** were confirmed using different spectroscopic methods. IR spectra characteristically revealed the existence of peaks for conjugated carbonyl groups at 1658 cm⁻¹. ¹H NMR spectra obviously showed two doublet signals corresponding to the vinyl protons CH=CH-CO with coupling constant 15.6–15.7 Hz indicating *trans* configuration^{46,47}. Also, ¹³C NMR spectra showed the presence of carbonyl carbon at δ 188.4–188.9 ppm along with *trans* olefinic carbons at δ 144.2–143.9 and δ 121.2–121.6 ppm.

A novel series of *N*-acetylpyrazolines **3a-f** was prepared in excellent yield (81–92%) by cyclocondensation of phenoxy halogenated chalcones **2a-f** using hydrazine hydrate in acetic acid as solvent⁴⁸. The characterisation of **3a-f** was conducted by IR spectra showing the presence of aliphatic CH at 2920–2978 cm⁻¹ and C=N peaks at 1589–1593 cm⁻¹, as well as disappearance of carbonyl group signals thus indicating the formation of a pyrazoline ring. The pyrazoline ring has a stereogenic carbon, thus compounds **3a-f** exist in two stereoisomers R and S. This was



Scheme 1. Synthesis of phenoxy halogenated chalcones **2a–f** and *N*-acetylpyrazolines **3a–f**. Reagents and conditions: (i) *p*-Substituted acetophenone, 40% KOH, 95% ethanol, 0 °C, (ii) Hydrazine hydrate, GAA, reflux 3 h.

obviously revealed by ¹H NMR spectra which verified the assigned structures of **3a–f** and showed clear characteristic signals of ABX spin system on the pyrazoline ring (Figure 3)^{49,50}. The two geminal protons of the pyrazoline ring resonated as two doublet of doublets at δ 3.12–3.16 ppm due to H_A of pyrazoline ring and at δ 3.83–3.85 ppm due to H_B of pyrazoline with geminal coupling constant of 18.0–18.4 Hz. On the other hand, the vicinal H_X pyrazoline proton appeared as a doublet of doublet at δ 5.54–5.56 ppm due to coupling with two magnetically non-equivalent protons with coupling constant of 4.4–4.6 Hz due to coupling with *trans* H_A and 11.8–12.0 Hz due to coupling with *cis* H_B. The CH₃ protons of the acetyl group were observed at δ 2.31–2.35 ppm in ¹H NMR spectra. ¹³C NMR spectra offered further evidence for *N*-acetylpyrazoline structure indicating the absence of *trans*-olefinic carbon signals and the presence of signals at δ 59.2–59.5 ppm corresponding for C5 pyrazoline and δ 42.3–42.5 ppm due to C4 of pyrazoline, in addition to a signal at δ 22.1–22.2 ppm due to CH₃ of the acetyl group.

Biological evaluation

Evaluation of anticancer activity

The synthesised chalcones **2a–f** and their corresponding *N*-acetylpyrazolines **3a–f** were evaluated for their anticancer activity against breast cancer cell line (MCF-7) and normal breast cell line (MCF-10a) using MTT assay protocol. The inhibitory concentration that exhibited 50% cell death (IC₅₀) was calculated for each compound as well as selectivity index for cancer cell line over normal cells. Staurosporine was used as reference drug. It is a kinase inhibitor and a strong inducer of apoptosis⁵¹. It was also reported as death inducer to MCF-7 human breast cancer cells^{52,53}. The results were displayed in Table 1.

In a closer look at Table 1, the IC₅₀ values on MCF-7 for the compounds can be used to explore structure activity relationship of the synthesised chalcones **2a–f** and their corresponding pyrazolines **3a–f** using staurosporine as reference drug (Figure 4).

For chalcone derivatives **2a–f**: the "R" substitution with bromo in the para position of diaryl ether moiety **2a–c** exhibited better activity than their chloro analogues **2d–f**. The IC₅₀ for 4-bromophenoxy derivatives ranged between 1.52–13.28 μ M with superior selectivity for compound **2c** of 15.24. On the other hand, 4-chlorophenoxy derivatives exhibited IC₅₀ values in the range of 1.87–44.20 μ M with selectivity index range of 0.5–11.03. What was noticed in this group of compounds is the same pattern of activity for substitutions in para position of the phenyl ring as derivatives with R¹ = CH₃ were the most active compounds **2c** and **2f** with IC₅₀ 1.52 and 1.87 μ M, respectively. The second place was occupied by the derivatives **2a** and **2d** having R¹ = Cl, while the least active derivatives were **2b** and **2e** with R¹ = Br (Figure 4).

For pyrazoline derivatives **3a–f**, phenoxy pyrazolines **3d–f** with R = Cl was more active than phenoxy pyrazolines **3a–c** with R = Br. The IC₅₀ for 4-chlorophenoxy pyrazoline derivatives **3d–f** ranged between 4.77–8.51 μ M with selectivity index range of 2.02–5.37. On the other hand, bromophenoxy derivatives **3a–c** exhibited IC₅₀ values in the range of 7.42–17.17 μ M with the existence of non-selective compound **3b**, with selectivity index of 0.67. Interestingly, the same pattern of activity for substitutions in para position of the phenyl ring that was noticed in chalcone derivatives was repeated in bromophenoxy pyrazolines where R¹ = CH₃ **3c** was the most active compound with IC₅₀ 7.42 μ M followed by derivatives with R¹ = Cl then derivatives with R¹ = Br. This pattern changed in one ranking position for 4-chlorophenoxy pyrazolines **3d–f** where the most active compound was again the derivative having R¹ = CH₃ **3f** with IC₅₀ 4.77 μ M followed by bromo analogue this time and finally the chloro derivative.

Literature survey revealed that, as pyrazoline ring is chiral, the activity of some biologically important pyrazoline compounds is due to one of the isomers, either R or S⁵⁴. However, in this study, pyrazoline derivatives **3a-f** were not as biologically interesting as the chalcone derivatives **2a-f**, thus no isomer separation was needed.

As an important point to discuss α,β -unsaturated compounds, as Michael acceptors, are of special interest due to their ability to undergo irreversible covalent interaction with MAPK leading to its inhibition⁵⁵. However, the possibility of being pan assay interference compounds (PAINS) may be an obstacle to many researchers. PAINS are considered as useless compounds in the drug discovery process as they show activity in multiple types of assays^{56,57}. However, in this study, it was found that the most active chalcone **2c** with methyl substituent at R¹ was 5.6-fold and 8.7-fold more active than its bioisosters **2a** and **2b**, respectively. Also chalcone **2f** with methyl substituent at R¹ was 10.6-fold and 23.6-fold more active than chalcones **2d** and **2e**, respectively. Moreover, the high selectivity index of compounds **2c** and **2f** excluded the doubt of being PAINS.

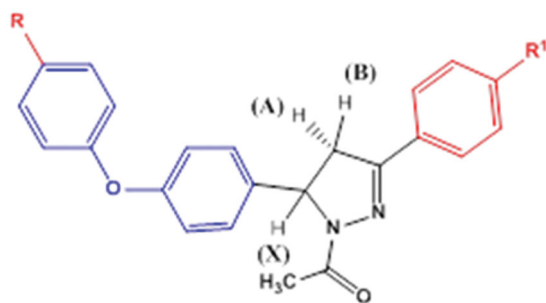


Figure 3. ABX spin system on the pyrazoline derivatives **3a-f**.

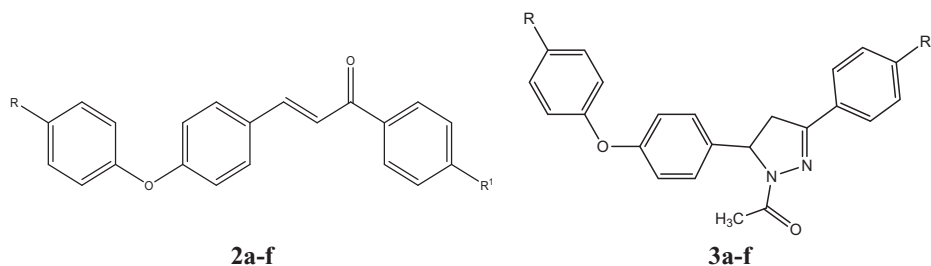
Cell cycle analysis

Anticancer agents exert their cytotoxic action by terminating cellular proliferation at definite checkpoints found at different stages of the cell cycle. Suppression of these phases results in the termination of the cell proliferation. Cell cycle analysis employs flow cytometry to differentiate between cells within different phases of the cell cycle. In this work, the effect of the most active compound **2c** on cell cycle progression was studied to explore the definite phase at which cell cycle arrest takes place in the MCF-7 breast cancer cell line. MCF-7 cells were treated with compound **2c** at its IC₅₀ concentration (1.52 μ M) and its effect on the cell population in different cell phases was recorded and displayed in Figure 5. Exposure of MCF-7 cells to compound **2c** resulted in significant decline in the cell population at the G₀/G₁ and S phases with 54.73% (from 55.05% to 24.92%) and 14.5% (from 34.18% to 29.22%), respectively. Moreover, marked augmentation was observed in the proportion of cells in the G₂/M phase by 4.25-fold, and in the pre-G₁ phase by 16.24-fold, in comparison to the control (DMSO). This clearly indicates that the target chalcone derivative **2c** arrested the cell cycle proliferation of MCF-7 cells in the G₂/M phase.

Annexin V-FITC apoptosis assay

Annexin V-FITC and Propidium iodide (PI) double-staining assay is a helpful method for determining whether cell death is due to programmed apoptosis or to uncontrolled necrosis. Dual staining for Annexin-V and PI permits discrimination between live cells, early apoptotic cells, late apoptotic cells and necrotic cells. Annexin V is a protein with high affinity for phosphatidylserine (PS). The latter is a cell membrane element that translocate from the inner face of the plasma membrane to the cell surface after initiating apoptosis. Once on the cell surface, PS can be detected

Table 1. *In vitro* anticancer screening against cancer cell line MCF-7 and normal cell line MCF-10a compared to staurosporine.



Compound	R	R ¹	<i>In vitro</i> cytotoxicity IC ₅₀ (μ M) ^a		
			MCF-7	MCF-10a	Selectivity index ^b
2a	Br	Cl	8.51 \pm 0.16	33.39 \pm 1.34	3.92
2b	Br	Br	13.28 \pm 0.53	25.33 \pm 1.17	1.91
2c	Br	CH ₃	1.52 \pm 0.03	23.16 \pm 0.88	15.24
2d	Cl	Cl	19.87 \pm 0.66	33.15 \pm 1.42	1.67
2e	Cl	Br	44.20 \pm 2.16	22.12 \pm 1.08	0.50
2f	Cl	CH ₃	1.87 \pm 0.02	20.63 \pm 0.37	11.03
3a	Br	Cl	10.56 \pm 0.39	55.82 \pm 1.92	5.29
3b	Br	Br	17.17 \pm 0.62	11.54 \pm 0.47	0.67
3c	Br	CH ₃	7.42 \pm 0.28	19.52 \pm 0.69	2.63
3d	Cl	Cl	8.51 \pm 0.27	45.74 \pm 1.36	5.37
3e	Cl	Br	5.02 \pm 0.22	10.12 \pm 0.62	2.02
3f	Cl	CH ₃	4.77 \pm 0.13	12.16 \pm 0.79	2.55
Staurosporine			5.90 \pm 0.14	15.33 \pm 0.51	2.60

^aIC₅₀ values are the mean \pm SD of three separate experiments.

^bSelectivity index was calculated as the ratio of cytotoxicity (IC₅₀) on normal cells (MCF-10a) to cancer cells (MCF-7).

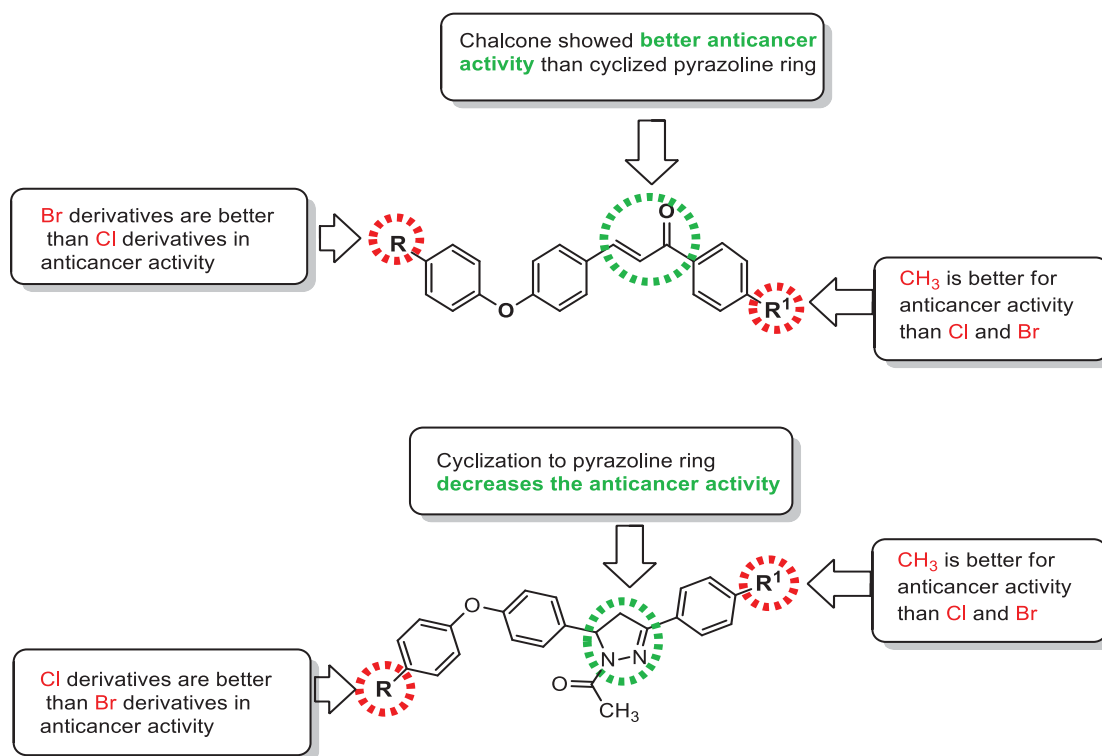


Figure 4. Structure activity relationship (SAR) of the synthesised chalcones **2a–f** and their cyclized derivatives *N*-acetylpyrazolines **3a–f**.

by fluorescent Annexin V conjugate. On the other hand, PI stains DNA and penetrates only dead cells⁵⁸. As shown in Figure 6, after 24 h of treatment of MCF-7 cells with compound **2c** at its IC₅₀ concentration (1.52 μM) a decrease in the percentage of the survived cells was detected. The results showed an increase in the apoptotic cells percentage in early apoptosis phase from 0.57% to 5.17% (9.0-fold more than control) and a significant elevation in late apoptosis phase from 0.38% to 21.96% (57.78-fold more than control) which merge on the intrinsic and extrinsic pathways. Moreover, this corresponds to an increase in the percentage of total apoptosis from 1.81% to 29.41% (16.24-fold, compared to the control).

Reactive oxygen species (ROS)

Reactive oxygen species (ROS) including superoxide anion (O₂⁻), hydroxyl radicals (HO[·]), and hydrogen peroxide (H₂O₂) are produced inside the cells as byproducts of metabolic processes. Moderate levels of ROS are beneficial to the cell and are used in the defending mechanisms against pathogenic infection as well as wound healing and repairing mechanisms⁵⁹. Normal healthy cells employ antioxidant defense system to detoxify extra ROS to maintain the balance between oxidant and antioxidant species⁶⁰. The oxidative stress occurs due to the accumulation of ROS in the cell when the production of ROS exceeds the ability of the cell to maintain the balance between its level and antioxidants. The accumulation of ROS can cause cell death due to its damaging effects on lipids, proteins and cellular DNA⁶¹. Moreover, the accumulation of ROS activates cellular pathways which affect cell proliferation, differentiation, and apoptosis including NF-κB and p38 MAPK pathways⁶². The anticancer activity of most chemotherapeutic agents is explained to be due to their ability to increase the level of ROS in cancer cells over a threshold to induce cell death⁶³.

The ability of many chalcone derivatives to act as pro-oxidant was documented in the literature⁶⁴. This action is thought to be linked to their cytotoxic behaviour in various cell lines⁶⁵. The induction of oxidative stress through production of ROS causes the damage of DNA and proteins. Production of phenoxide radicle of chalcone derivatives may constitute the main ROS agent⁶⁶. In this investigation and as a result of the existence of phenoxy moiety in the synthesised chalcone derivatives, ROS production of compound **2c** was evaluated on MCF-7 cell line using 1.52 μM and the results were displayed in Figure 7. As a result of this evaluation, compound **2c** can induce ROS by 10% higher than control in MCF-7 cells.

Evaluation of p38 MAPK

The p38 MAPK is one group of kinase family with a critical role in cancer progression⁶⁷. Down-regulation of this enzyme was associated with diminished survival of breast cancer cells⁶⁸. In a previous study, Parekh et al. observed that liver cancer cell development has high p38 and after using resveratrol both total and phosphorylated p38 were down-regulated⁶⁹. Down-regulation of p38 MAPK regulates cell apoptosis and oxidative stress by expression of pro-inflammatory and G2/M checkpoint regulation leading to DNA damage which decrease cancer growth and invasiveness⁷⁰.

The concentration of phosphorylated and total p38 MAPK was evaluated in MCF-7 cells using 1.52 μM of compound **2c** to assess its ability to down-regulate this key enzyme. The results indicated that compound **2c** can down-regulate total p38 MAPK by almost 40% and can interfere with its phosphorylation by almost 60% (Figure 8). Compound **2c** decreased both total p38 MAPK (p38T, Figure 8) and phosphorylated p38 MAPK (p38P, Figure 8) in MCF-7 treated cells when compared to untreated MCF-7 cells which suggests that compound **2c** caused inhibition of cell proliferation,

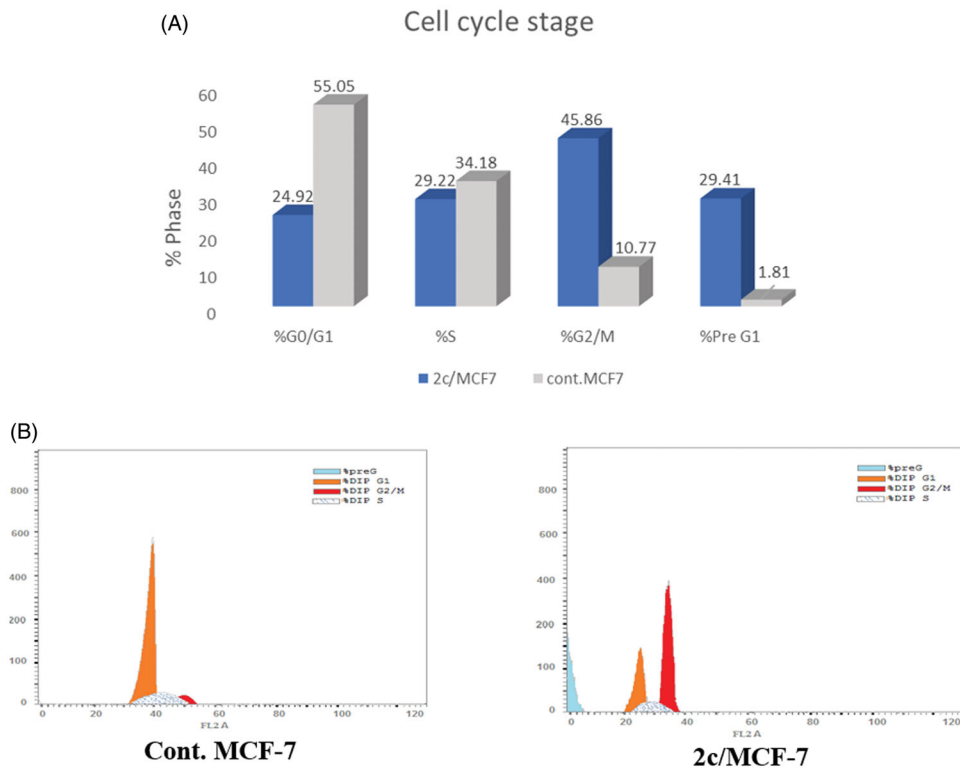


Figure 5. (A) Graphical representation of the effect of compound 2c on the cell cycle stages of MFC-7 cells. (B) Effect of compound 2c (1.52 μ M) on DNA-ploidy flow cytometric analysis of MFC-7 cells after 24 h.

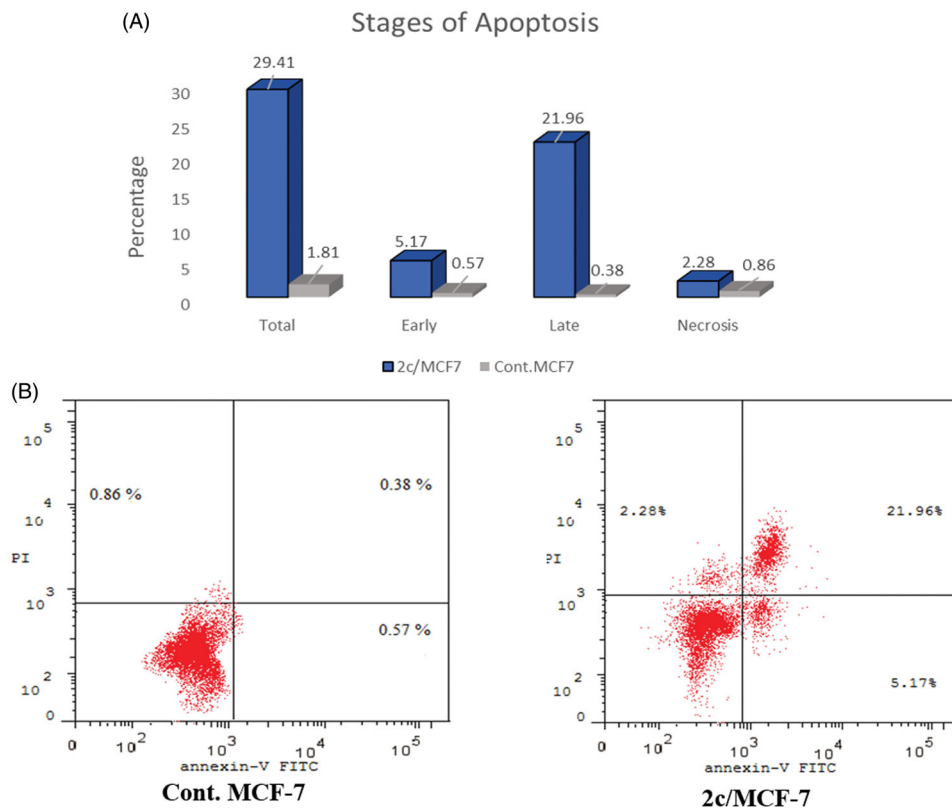


Figure 6. (A). Percentage and stages of induced apoptosis in control MFC-7 and MFC-7 treated with compound 2c. (B) Representative dot plots of MFC-7 cells treated with 2c (1.52 μ M) for 24 h and analysed by flow cytometry after double staining of the cells with Annexin-V-FITC and PI.

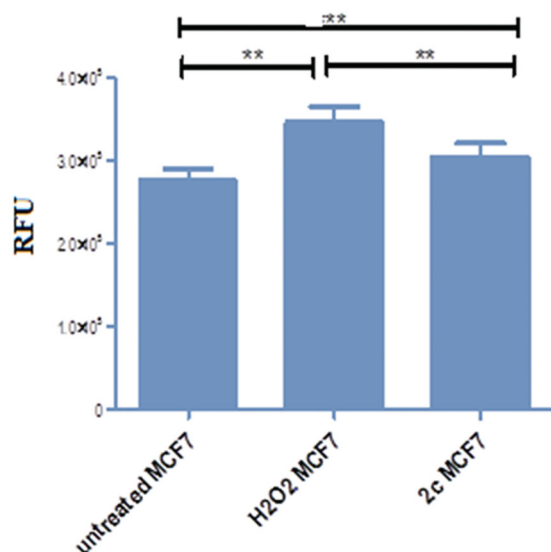


Figure 7. Graphical representation to show the increase of intercellular ROS in 2c treated MCF-7 cells compared to H₂O₂ treated MCF-7 and untreated MCF-7 cells. ROS content was reported as relative fluorescence units (RFU).

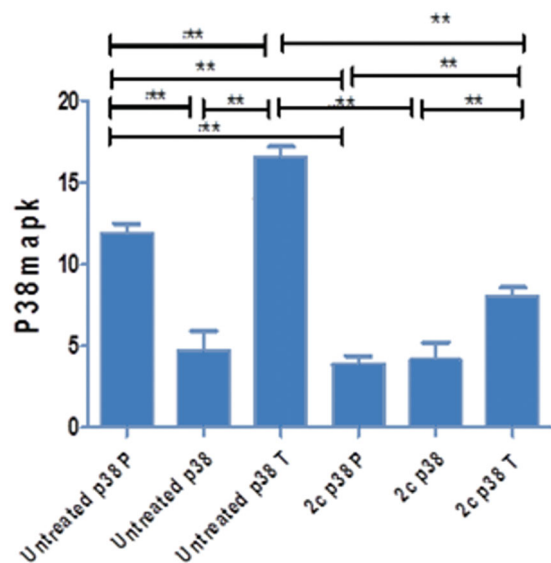


Figure 8. Graphical representation to show that 2c treated MCF-7 cells decreased both total p38 MAPK (p38T) and phosphorylated p38 MAPK (p38P) compared to untreated MCF-7 cells.

growth, and survival. Down-regulation of p38 MAPK as well as induction of ROS production may explain the cytotoxic activity of compound **2c**.

Molecular docking study

In the search for the possible mechanism of the compounds in inhibition of p38 MAPK pathway, chalcones **2c** and **2f** that showed the best IC₅₀ values against MCF-7 cell line were docked to the crystal structure of p38alpha MAP kinase complexed with [5-amino-1-(4-fluorophenyl)-1H-pyrazol-4-yl][3-(piperidin-4-yloxy)phenyl]methanone (PQA) ligand (PDB code: 2BAL)⁴² using MOE, 2019.0102 software. Through examination of the binding interactions of PQA to the active site of the enzyme, it shows strong

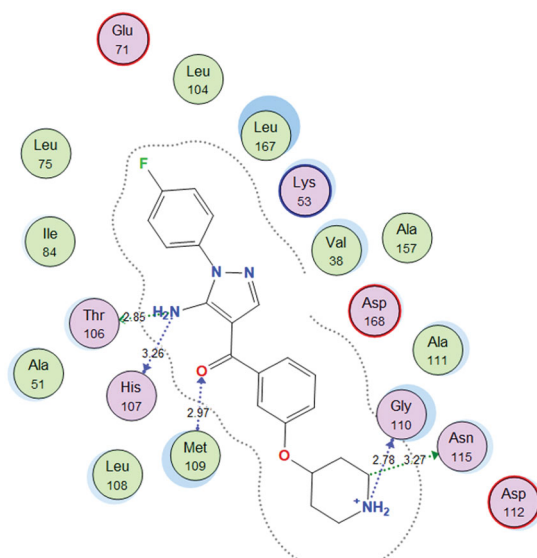


Figure 9. 2D interactions of PQA within p38alpha MAP kinase active site.

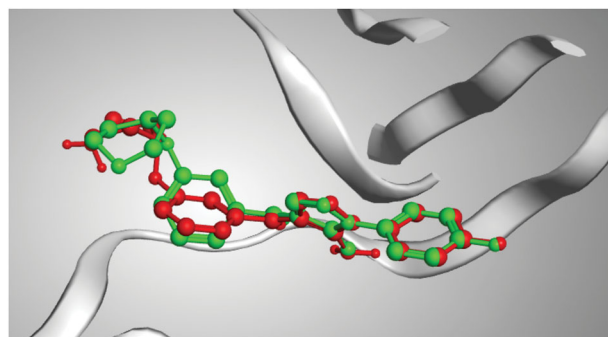


Figure 10. 3D representation of the superimposition of the co-crystallised (red) and the docking pose (green) of PQA in the active site of p38alpha MAP kinase enzyme.

Table 2. Docking scores, hydrogen bonds and interactions of tested compounds **2c** and **2f** inside p38alpha MAP kinase binding site (PDB entry 2BAL).

Compound	S (kcal/mol)	Amino acids	Interacting groups	Type of interaction	Length
2c	-11.5298	Lys53	O (C=O)	H-bond acceptor	3.00
		Met109	O (Ether)	H-bond acceptor	3.36
2f	-11.3114	Lys53	O (C=O)	H-bond acceptor	3.12
		Met109	O (Ether)	H-bond acceptor	3.27

hydrogen bond interactions with Thr106, His107, Met109 & Gly110 (Figure 9).

Docking setup was first validated by self-docking of the co-crystallised ligand (PQA) in the vicinity of the binding site of the enzyme, the docking score (S) was -11.9710 kcal/mol. and root mean square deviation (RMSD) was 1.7685 Å (Figure 10).

Both tested compounds **2c** and **2f** showed good binding energy score which is similar to the bound ligand (-11.5298 and -11.3114 kcal/mol., respectively). They showed binding interactions with Lys53 and the key amino acid Met109. Moreover, they showed good fitting in the enzyme pocket which is clarified in the 3D pictures of the best docking poses. The results are summarised in Table 2 and Figures 11 and 12).

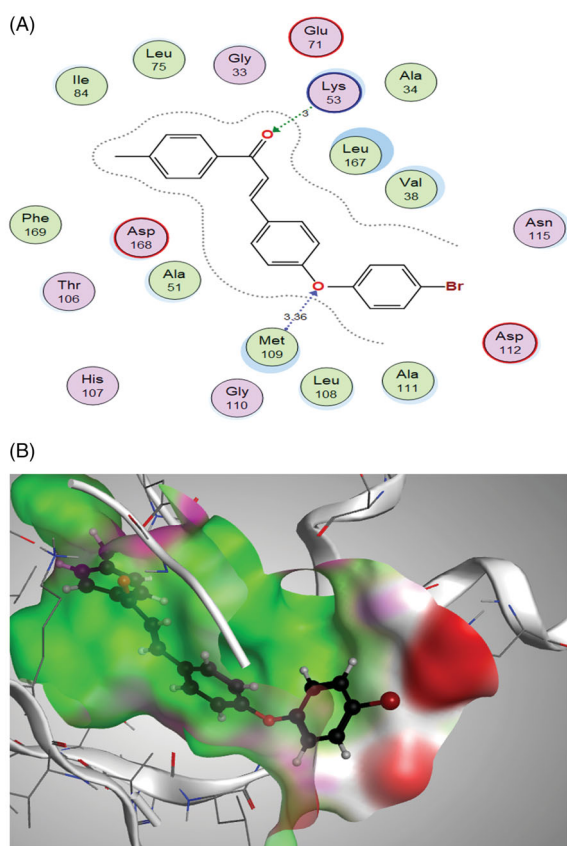


Figure 11. (A) 2D interactions of compound 2c within p38alpha MAP kinase active site; (B) 3D diagram of compound 2c interactions within p38alpha MAP kinase active site.

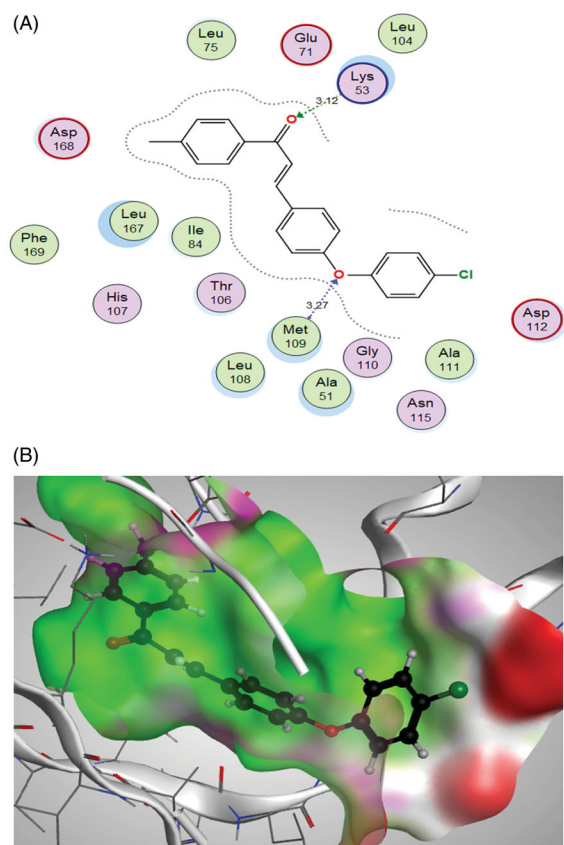


Figure 12. (A) 2D interactions of compound 2f within p38alpha MAP kinase active site; (B) 3D diagram of compound 2f interactions within p38alpha MAP kinase active site.

Conclusion

A series of halogenated phenoxychalcones **2a–f** and their corresponding *N*-acetylpyrazolines **3a–f** was synthesised and evaluated for their anticancer activity against MCF-7 breast cancer cell line. The synthesised compounds showed significant cytotoxic activity and the most promising was compound **2c** with IC_{50} of $1.52 \mu\text{M}$ and 15-fold selectivity towards breast cancer cell line over normal breast cell line. Compound **2c** down-regulated p38 α MAPK and induced ROS in MCF-7 cell line. Direct interaction of compound **2c** with p38alpha MAP Kinase active sites was revealed by molecular docking studies. It also caused cell cycle arrest in G2/M phase which indicates its apoptotic behaviour. The same compound induced significant increase in apoptotic cells in late apoptosis phase by 57.78-fold when compared to control. The investigation of chemical modifications of the chalcone structure by introducing electron withdrawing, meta directing groups such as nitro group in different positions would be of great value. Furthermore, the evaluation of the anti-tubulin polymerisation of the synthesised diaryl ether chalcones would be of great importance for better understanding of the biological activity.

Acknowledgements

The authors thank Dr. Esam Rashwan, Head of the confirmatory diagnostic unit VACSERA-EGYPT, for carrying out cytotoxicity screening, cell cycle analysis, evaluation of ROS and p38 MAPK.

Disclosure statement

The authors declare that they have no conflicts of interest. The authors alone are responsible for the content and writing of this manuscript.

Funding

The author(s) reported there is no funding associated with the work featured in this article.

References

- Boström J, Brown DG, Young RJ, Keserü GM. Expanding the medicinal chemistry synthetic toolbox. *Nat Rev Drug Discov* 2018;17:709–27.
- Singh I, Rani R, Luxami V, Paul K. Synthesis of 5-(4-(1H-phenanthro[9,10-d]imidazol-2-yl)benzylidene)thiazolidine-2,4-dione as promising DNA and serum albumin-binding agents and evaluation of antitumor activity. *Eur J Med Chem* 2019; 166:267–80.
- El-dash Y, Elzayat E, Abdou AM, Hassan RA. Novel thienopyrimidine-aminothiazole hybrids: design, synthesis, antimicrobial screening, anticancer activity, effects on cell cycle profile, caspase-3 mediated apoptosis and VEGFR-2 inhibition. *Bioorganic Chemistry* 2021;114:105137.
- Caruso E, Malacarne MC, Marras E, et al. New BODIPYs for photodynamic therapy (PDT): synthesis and activity on human cancer cell lines. *Bioorg Med Chem* 2020;28:115737.
- Kassab AE, Gedawy EM, Hamed MIA, et al. Design, synthesis, anticancer evaluation, and molecular modelling studies of novel tolmetin derivatives as potential VEGFR-2 inhibitors and apoptosis inducers. *J Enzyme Inhib Med Chem* 2021;36: 922–39.

6. El-Malah A, Mahmoud Z, Hamed Salem H, Abdou AM, et al. Design, ecofriendly synthesis, anticancer and antimicrobial screening of innovative *Biginelli dihydropyrimidines* using β -aroylpyruvates as synthons. *Green Chem Lett Rev* 2021;14:220–32.
7. Sung H, Ferlay J, Siegel RL, et al. Global cancer statistics 2020: GLOBOCAN estimates of incidence and mortality worldwide for 36 cancers in 185 countries. *CA Cancer J Clin* 2021;71:209–49.
8. Fikroh RA, Matsjeh S, Anwar C, et al. Synthesis and anticancer activity of (E)-2'-hydroxy-2-bromo-4,5-dimethoxychalcone against breast cancer (MCF-7) cell line. *Molekul* 2020;15:34–9.
9. Rammohan A, Reddy JS, Sravya G, et al. Chalcone synthesis, properties and medicinal applications: a review. *Environ Chem Lett* 2020;18:433–58.
10. Sukumaran SD, Nasir SB, Tee JT, et al. Analogues of 2'-hydroxychalcone with modified C4-substituents as the inhibitors against human acetylcholinesterase. *J Enzyme Inhib Med Chem* 2021;36:130–7.
11. Emam SH, Sonousi A, Osman EO, et al. Design and synthesis of methoxyphenyl- and coumarin-based chalcone derivatives as anti-inflammatory agents by inhibition of NO production and down-regulation of NF- κ B in LPS-induced RAW264.7 macrophage cells. *Bioorg Chem* 2021;107:104630.
12. Dan W, Dai J. Recent developments of chalcones as potential antibacterial agents in medicinal chemistry. *Eur J Med Chem* 2020;187:111980.
13. Sashidhara KV, Dodda RP, Sonkar R, Palnati GR, et al. Design and synthesis of novel indole-chalcone fibrates as lipid lowering agents. *Eur J Med Chem* 2014;81:499–509.
14. Wang G, Liu W, Gong Z, et al. Synthesis, biological evaluation, and molecular modelling of new naphthalene-chalcone derivatives as potential anticancer agents on MCF-7 breast cancer cells by targeting tubulin colchicine binding site. *J Enzyme Inhib Med Chem* 2020;35:139–44.
15. Ashour HF, Abou-zeid LA, El-Sayed MAA, Selim KB. 1,2,3-triazole-chalcone hybrids: synthesis, in vitro cytotoxic activity and mechanistic investigation of apoptosis induction in multiple myeloma RPMI-8226. *Eur J Med Chem* 2020;189:112062.
16. Chouiter MI, Boulebd H, Pereira DM, et al. New chalcone-type compounds and 2-pyrazoline derivatives: synthesis and caspase-dependent anticancer activity. *Future Med Chem* 2020;12:493–509.
17. Bedos-Belval F, Rouch A, Vanucci-Bacqué C, Baltas M. Diaryl ether derivatives as anticancer agents – a review. *Medchemcomm* 2012;3:1356–72.
18. Pitsinos EN, Vidali VP, Couladouros EA. Diaryl ether formation in the synthesis of natural products. *Eur J Org Chem* 2011;2011:1207–22.
19. Yang SM, Huang ZN, Zhou ZS, et al. Structure-based design, structure-activity relationship analysis, and antitumor activity of diaryl ether derivatives. *Arch Pharm Res* 2015;38:1761–73.
20. Wang G, Liu W, Gong Z, et al. Design, synthesis, biological evaluation and molecular docking studies of new chalcone derivatives containing diaryl ether moiety as potential anticancer agents and tubulin polymerization inhibitors. *Bioorg Chem* 2020;95:103565.
21. Zhang H, Liu JJ, Sun J, et al. Design, synthesis and biological evaluation of novel chalcone derivatives as antitubulin agents. *Bioorg Med Chem* 2012;20:3212–8.
22. Kurşun Aktar BS, ORUÇ-EMRE EE, Demirtas I, et al. Synthesis and biological evaluation of novel chalcones bearing morpholine moiety as antiproliferative agents. *Turkish J Chem* 2018;42:482–92.
23. Dahlen K, Wallen EA, Grøtli M, Luthman K. Synthesis of 2,3,6,8-tetrasubstituted chromone scaffolds. *J Org Chem* 2006;71:6863–71.
24. Dyrager C, Friberg A, Dahlén K, et al. 2,6,8-Trisubstituted 3-hydroxychromone derivatives as fluorophores for live-cell imaging. *Chemistry* 2009;15:9417–23.
25. Dias TA, Duarte CL, Lima CF, et al. Superior anticancer activity of halogenated chalcones and flavonols over the natural flavonol quercetin. *Eur J Med Chem* 2013;65:500–10.
26. Jain UK, Bhatia RK, Rao AR, et al. Design and development of halogenated chalcone derivatives as potential anticancer agents. *Trop J Pharm Res* 2014;13:73–80.
27. Bilginer S, Gul HI, Erdal FS, et al. New halogenated chalcones with cytotoxic and carbonic anhydrase inhibitory properties: 6-(3-Halogenated phenyl-2-propen-1-oyl)-2(3H)-benzoxazolones. *Arch Pharm* 2020;353:1900384–8.
28. Schmitt F, Draut H, Biersack B, Schobert R. Halogenated naphthochalcones and structurally related naphthopyrazolines with antitumor activity. *Bioorg Med Chem Lett* 2016;26:5168–71.
29. Saavedra E, Del Rosario H, Brouard I, et al. '6'-Benzyloxy-4-bromo-2'-hydroxychalcone is cytotoxic against human leukaemia cells and induces caspase-8- and reactive oxygen species-dependent apoptosis. *Chem Biol Interact* 2019;298:137–45.
30. dos Santos MB, Bertholin Anselmo D, de Oliveira JG, et al. Antiproliferative activity and p53 upregulation effects of chalcones on human breast cancer cells. *J Enzyme Inhib Med Chem* 2019;34:1093–9.
31. Pontes O, Costa M, Santos F, et al. Exploitation of new chalcones and 4H-chromenes as agents for cancer treatment. *Eur J Med Chem* 2018;157:101–14.
32. Reddy Kotha R, G Kulkarni R, Garige AK, et al. Synthesis and cytotoxic activity of new chalcones and their flavonol derivatives. *Med Chem* 2017;7:353–60.
33. Fayed EA, Eldin RRE, Mehany A, et al. Isatin-Schiff's base and chalcone hybrids as chemically apoptotic inducers and EGFR inhibitors; design, synthesis, anti-proliferative activities and in silico evaluation. *J Mol Struct* 2021;1234:130159.
34. Abdelhafez OM, Ahmed EY, Abdel Latif NA, et al. Design and molecular modeling of novel P38 α MAPK inhibitors targeting breast cancer, synthesized from oxygen heterocyclic natural compounds. *Bioorg Med Chem* 2019;27:1308–19.
35. Bradham C, McClay DR. p38 MAPK in development and cancer. *Cell Cycle* 2006;5:824–8.
36. Sharma R, Kumar R, Kodwani R, et al. A review on mechanisms of anti tumor activity of chalcones. *Anticancer Agents Med Chem* 2015;16:200–11.
37. Matiadis D, Sagnou M. Pyrazoline hybrids as promising anticancer agents: an up-to-date overview. *Int J Mol Sci* 2020;21:1–41.
38. Zheng X, Ding J, Chen J, et al. The coupling of arylboronic acids with nitroarenes catalyzed by rhodium. *Org Lett* 2011;13:1726–9.
39. Kumar P, Tripathi L. A new class of anticonvulsants possessing 6Hz psychomotor seizure test activity: 2-(1H-benzotriazol-1-yl)-N'-[substituted] acetohydrazides. *Med Chem* 2012;8:337–48.

40. Scudiero DA, Shoemaker RH, Paull KD, et al. Evaluation of a soluble tetrazolium/formazan assay for cell growth and drug sensitivity in culture using human and other tumor cell lines. *Cancer Res* 1988;48:4827–33.
41. Tolba MF, Esmat A, Al-Abd AM, et al. Caffeic acid phenethyl ester synergistically enhances docetaxel and paclitaxel cytotoxicity in prostate cancer cells. *IUBMB Life* 2013;65:716–29.
42. Sullivan JE, Holdgate GA, Campbell D, et al. Prevention of MKK6-dependent activation by binding to p38alpha MAP kinase. 2005;44:16475–90.
43. RCSB PDB. <https://www.rcsb.org/structure/2BAL>.
44. Pambudi W, Haryadi W, Matsjeh S, Indarto I. The effectiveness of hydroxychalcone synthesis by using NaOH and NaOH + ZrO₂ montmorillonite catalyst through conventional and microwave assisted organic synthesis (Maos) method. *J Phys Conf Ser* 2019;1155:12074.
45. Sivasankerreddy L, Nagamani B, Rajkumar T, et al. Novel diazenyl containing phenyl styryl ketone derivatives as antimicrobial agents. *Anti-Infective Agents* 2019;17:28–38.
46. Simmler C, Lankin DC, Nikolić D, et al. Isolation and structural characterization of dihydrobenzofuran congeners of licochalcone A. *Fitoterapia* 2017;121:6–15.
47. Xiao Y, Han F, Lee IS. Microbial transformation of licochalcones. *Molecules* 2019;25:60.
48. Hassan SY. Synthesis and biological activity of some new pyrazoline and pyrimidine derivatives. *J Braz Chem Soc* 2011;22:1286–98.
49. Karabacak M, Altıntop MD, Çiftçi HI, et al. Synthesis and evaluation of new pyrazoline derivatives as potential anti-cancer agents. *Molecules* 2015;20:19066–84.
50. Suma AAT, Wahyuningsih TD, Pranowo D. Synthesis and antibacterial activities of n-phenylpyrazolines from veratraldehyde. *Mater Sci Forum* 2017;901:124–32.
51. Jiang Y, Cai NN, Zhao XX, et al. Decreased abundance of GDNF mRNA transcript in the immature Sertoli cells of cattle in response to protein kinase inhibitor staurosporine. *Anim Reprod Sci* 2020;214:1–9.
52. Xue LY, Chiu SM, Oleinick NL. Staurosporine-induced death of MCF-7 human breast cancer cells: a distinction between caspase-3-dependent steps of apoptosis and the critical lethal lesions. *Exp Cell Res* 2003;283:135–45.
53. Alsamman K, El-Masry OS. Staurosporine alleviates cisplatin chemoresistance in human cancer cell models by suppressing the induction of SQSTM1/p62. *Oncol Rep* 2018;40:2157–62.
54. Goksen US, Sarigul S, Bultinck P, et al. Absolute configuration and biological profile of pyrazoline enantiomers as MAO inhibitory activity. *Chirality* 2019;31:21–33.
55. Wei L, Wu J, Li G, Shi N. Cis-enone resorcylic acid lactones (RALs) as irreversible protein kinase inhibitors. *Curr Drug Metab* 2012;18:1186–98.
56. Baell JB, Holloway GA. New substructure filters for removal of pan assay interference compounds (PAINS) from screening libraries and for their exclusion in bioassays. *J Med Chem* 2010;53:2719–40.
57. Mendgen T, Steuer C, Klein CD. Privileged scaffolds or promiscuous binders: a comparative study on rhodanines and related heterocycles in medicinal chemistry. *J Med Chem* 2012;55:743–53.
58. Vermes I, Haanen C, Steffens-Nakken H, Reutelingsperger C. A novel assay for apoptosis flow cytometric detection of phosphatidylserine expression on early apoptotic cells using fluorescein labelled Annexin V. *J Immunol Methods* 1995;184:39–51.
59. Bhattacharyya A, Chattopadhyay R, Mitra S, Crowe SE. Oxidative stress: an essential factor in the pathogenesis of gastrointestinal mucosal diseases. *Physiol Rev* 2014;94:329–54.
60. He L, He T, Farrar S, et al. Antioxidants maintain cellular redox homeostasis by elimination of reactive oxygen species. *Cell Physiol Biochem* 2017;44:532–53.
61. Acharya A, Das I, Chandhok D, Saha T. Redox regulation in cancer: a double-edged sword with therapeutic potential. *Oxid Med Cell Longev* 2010;3:23–34.
62. Wang Z, Li S, Cao Y, et al. Oxidative stress and carbonyl lesions in ulcerative colitis and associated colorectal cancer. *Oxid Med Cell Longev* 2016;2016:9875298.
63. Kong Q, Beel JA, Lillehei KO. A threshold concept for cancer therapy. *Med Hypotheses* 2000;55:29–35.
64. Strathmann J, Klimo K, Sauer SW, et al. Xanthohumol-induced transient superoxide anion radical formation triggers cancer cells into apoptosis via a mitochondria-mediated mechanism. *FASEB J* 2010;24:2938–50.
65. Takac P, Kello M, Vilkova M, et al. Antiproliferative effect of acridine chalcone is mediated by induction of oxidative stress. *Biomolecules* 2020;10:345.
66. Martindale JL, Holbrook NJ. Cellular response to oxidative stress: signaling for suicide and survival. *J Cell Physiol* 2002;192:1–15.
67. Tsai PW, Shiah SG, Lin MT, et al. Up-regulation of vascular endothelial growth factor C in breast cancer cells by heregulin-beta 1. A critical role of p38/nuclear factor-kappa B signaling pathway. *J Biol Chem* 2003;278:5750–9.
68. Suarez-Cuervo C, Merrell MA, Watson L, et al. Breast cancer cells with inhibition of p38alpha have decreased MMP-9 activity and exhibit decreased bone metastasis in mice. *Clin Exp Metastasis* 2004;21:525–33.
69. Parekh P, Motiwale L, Naik N, Rao KVK. Downregulation of cyclin D1 is associated with decreased levels of p38 MAP kinases, Akt/PKB and Pak1 during chemopreventive effects of resveratrol in liver cancer cells. *Exp Toxicol Pathol* 2011;63:167–73.
70. Soni S, Anand P, Padwad YS. MAPKAPK2: the master regulator of RNA-binding proteins modulates transcript stability and tumor progression. *J Exp Clin Cancer Res* 2019;38:121.